Focusing of ultrasonic waves by negative refraction in phononic crystals

J. H. Page

Citation: AIP Advances **6**, 121606 (2016); doi: 10.1063/1.4972204
View online: http://dx.doi.org/10.1063/1.4972204
View Table of Contents: http://aip.scitation.org/toc/adv/6/12
Published by the American Institute of Physics

AIP ADVANCES **6**, 121606 (2016)

Focusing of ultrasonic waves by negative refraction in phononic crystals

J. H. Page[a,b]
Department of Physics and Astronomy, University of Manitoba, Winnipeg, Manitoba, R3T 2N2, Canada

(Received 11 October 2016; accepted 29 November 2016; published online 19 December 2016)

Negative refraction and focusing phenomena in phononic crystals is reviewed, starting with their initial discovery over 10 years ago in flat three-dimensional (3D) phononic crystals. This work soon led to direct observations of negative refraction in 2D phononic crystals, and an extensive series of experiments, simulations and theoretical predictions to explore and optimize focusing by flat phononic crystal lenses. More recently, the emphasis has been on demonstrating how super-resolution focusing that beats the diffraction limit can be achieved. Ultrasonic experiments, in combination with theory and simulations, have played an important role in developing a detailed understanding of these phenomena. [http://dx.doi.org/10.1063/1.4972204]

I. INTRODUCTION

The focusing of phonons and acoustic waves in crystals has a long history that predates the recent interest in phononic crystals. The phenomenon called "phonon focusing" started with observations that heat flux in the low temperature ballistic transport regime of atomic crystals is channeled along particular directions due to elastic anisotropy.[1] Since this phonon focusing effect is observed at long wavelengths compared with the lattice constants of atomic crystals, continuum elasticity can be used to explain the experiments. Phonon focusing occurs because in elastically anisotropic media, the group velocity $\mathbf{v_g}$ and wavevector $\mathbf{k}$ are not parallel in general, with the result that waves with different $\mathbf{k}$ can have similar $\mathbf{v_g}$, and the energy flux, which follows the direction of the group velocity, is therefore channeled along certain crystalline directions. This focusing effect has been observed in a wide variety of experiments, from heat pulse transport to ultrasonic propagation from a point-like source, with the experimental evidence and physical interpretation being comprehensively reviewed in the book by J.P. Wolfe.[2]

During the explosion of activity in phononic crystal research at the end of the 1990s and early 2000s, it therefore seemed natural to ask whether interesting and possibly different focusing and imaging phenomena could occur in phononic crystals. About this time, it became widely recognized that doubly negative materials, with simultaneously negative electric permittivity and magnetic permeability for electromagnetic waves, or with negative modulus and mass density for acoustic waves, have a negative refractive index, with the Poynting vector ($\propto \mathbf{v_g}$) and $\mathbf{k}$ pointing in opposite directions. At the interface between positive and doubly negative materials, waves are therefore refracted negatively, which is the basis of Pendry's "perfect lens".[3] My group was curious to see if focusing by negative refraction could also be observed in phononic crystals, in this case due to the effects of

[a]Electronic mail: john.page@umanitoba.ca

[b]At the Phononics 2015 conference, John Page, Suxia Yang and Zhengyou Liu were awarded the 2015 Brillouin Medal for the "first demonstration of focusing of acoustic waves by negative refraction in a flat phononic crystal". This paper draws on material presented in the Brillouin Lecture at this conference, and reviews the very active area of research on negative refraction and focusing of acoustic waves in phononic crystals that has developed since this initial demonstration, starting with a summary of the main results from the first paper on this topic.

Bragg scattering on the crystal's band structure, which might cause $\mathbf{v_g}$ and $\mathbf{k}$ to point in different directions, and perhaps even be of opposite sign.

In this paper, I review the research on negative refraction and focusing in phononic crystals that was initiated by the first ultrasonic experiments to explore these phenomena.[4] These experiments capitalized on the ability to construct high quality 3D and 2D phononic crystals and to use the versatility of ultrasonic techniques to measure phononic crystal properties with excellent resolution in space, time and frequency. The review begins with the initial work on focusing in a 3D phononic crystal, and then summarizes more recent work by many groups on negative refraction and super-resolution focusing, mainly in 2D phononic crystals. The article ends with a perspective on future research.

II. FOCUSING OF ULTRASOUND IN A 3D PHONONIC CRYSTAL

Experiments performed on a three-dimensional phononic crystal consisting of 0.800-mm-diameter tungsten-carbide beads immersed in water were the first to demonstrate the focusing of ultrasonic waves by negative refraction,[4] initiating a new direction in phononic crystal research that has been very active over the last decade,[5,6] and continues to attract considerable attention, especially now for acoustic metamaterials. The beads were carefully arranged in a close-packed face-centered-cubic structure, with the crystal used in these focusing experiments consisting of a 12-layer-thick slab in which the [111] or ΓL direction was perpendicular to the layers. The crystal was supported on a substrate, which was sufficiently thick so that any echoes reverberating back and forth in the substrate would delayed long enough not to contaminate the main signal. In this crystal, focusing effects were discovered at frequencies near 1.6 MHz in the third pass band of the crystal's band structure [Fig. 1(a)], well above the first complete band gap that occurs between 0.98 and 1.2 MHz.[7] Along the ΓL direction in this third band, the wave vector and group velocity have opposite sign, suggesting that in this frequency range behaviour analogous to negative refraction focusing in doubly negative materials could occur. In the experiments (see Fig. 1(b) for a schematic diagram of the setup), a small point-like source consisting of a pinducer (radius $\sim\lambda$, where λ is the wavelength in water) was placed near the sample surface at a distance of 3 mm (approximately 3λ at 1.6 MHz). The pulse emitted by the pinducer was transmitted through the crystal and its substrate, and then detected by a small hydrophone (diameter $<< \lambda$) placed 3 mm below the substrate. The hydrophone was scanned over a closely-spaced grid of points in a plane parallel to the crystal surface to measure the transmitted field as a function of position and time. By taking the Fourier transforms of each transmitted pulse, the amplitude of the transmitted field for each frequency in the bandwidth of the pulse was determined, thereby enabling the spatial field pattern in the measurement plane to be determined at all of the accessible frequencies. The field pattern was found to be strongly dependent on frequency, due to the large changes with frequency in the anisotropy of the dispersion relation in this band, as can be seen in Fig. 1(a). At 1.57 MHz, the measured field pattern in the detection plane showed a tightly focused spot with a FWHM of only 5 mm, as shown in Fig. 1(c). The focal spot is more than 10 times narrower than the beam from the pinducer without the crystal in place, this diverging beam having spread out at this frequency to a FWHM in the detection plane of 65 mm (more than three quarters of the width of the region imaged in the figure). Thus, the possibility of focusing ultrasonic waves using a phononic crystal with flat parallel faces was clearly demonstrated by this example. It is worth noting that, in this case, the image of the source is formed deep in the far field, with the crystal-to-image distance being approximately 130 wavelengths; subsequent work has shown that it is unusual to achieve good far field focusing with a phononic crystal "lens", so that this result may be viewed as a quite remarkable feature of these initial focusing data.

To understand the origin of the focusing effect, it is instructive to examine the equifrequency surfaces, which, at a given frequency, represent the variation with direction of the magnitude of the wave vector. Figure 1(e) shows cross sections at several frequencies of the 3D equifrequency surfaces in a plane containing the [111] direction. The equifrequency surfaces were calculated using the Multiple Scattering Theory (MST),[8] and their cross sections are plotted in Fig. 1(e) in the reduced zone scheme. For comparison, the circular cross section of the equifrequency surface for water at 1.6 MHz

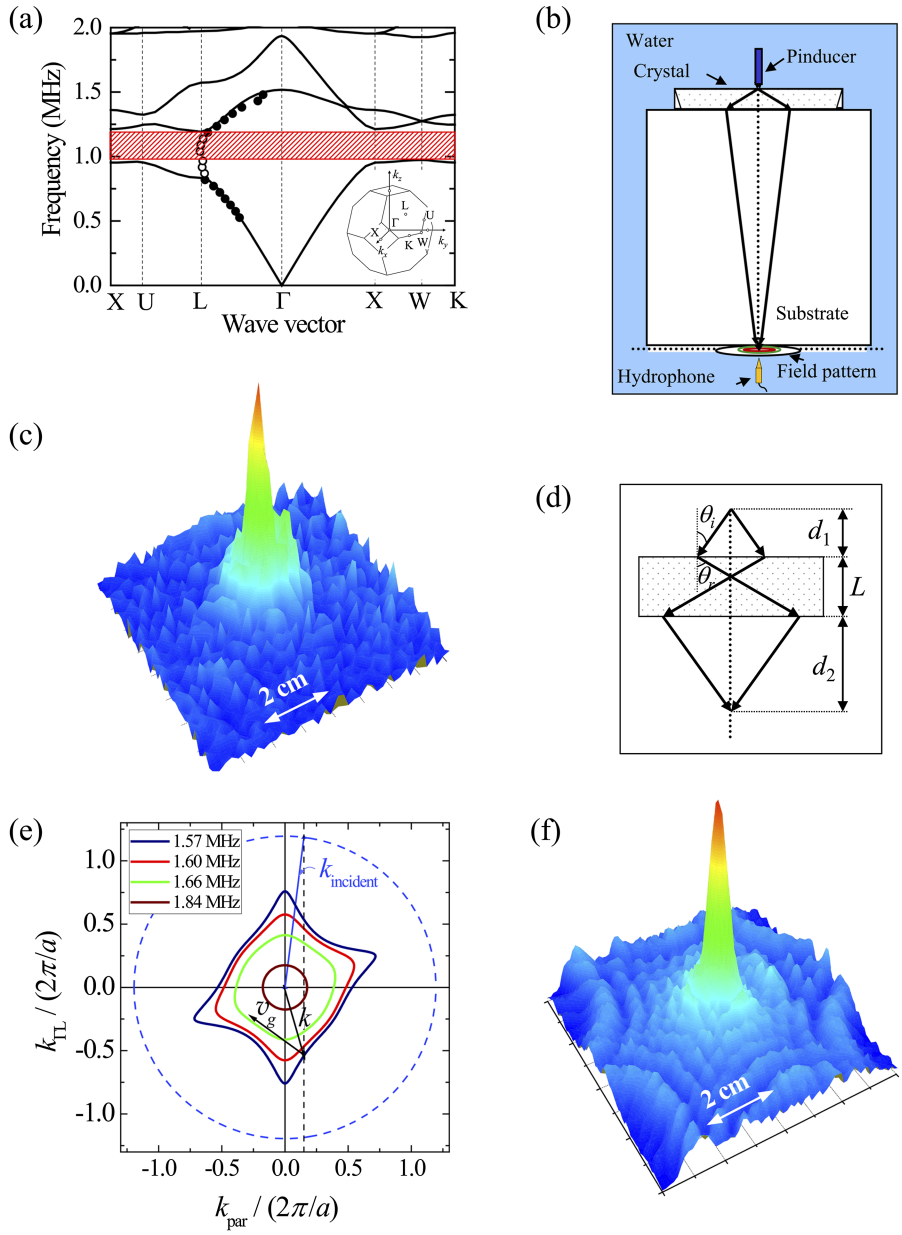

FIG. 1. (a) Band structure of the fcc crystal of tungsten carbide beads in water. The high symmetry points of the Brillouin zone are indicated in the inset. The red hatched area delineates the first complete band gap. (b) Schematic diagram illustrating the experimental setup. The arrows between the source and detector depict typical "rays" indicating the directions of the group velocity for a representative pair of plane wave components of the input field. (c) Image of the source focused by the 12-layer crystal. (d) The focusing condition for a negative index medium with no substrate. (e) Cross sections of the equifrequency surfaces of this phononic crystal at several frequencies in a plane containing the [111], [110] and [001] directions, with the [111] direction being along the y axis. The dashed circle is the equifrequency contour for water at 1.6 MHz. The dashed vertical black line is drawn to indicate the value of $\mathbf{k}_{par}$ that satisfies Snell's law for a representative incident plane wave with wave vector $\mathbf{k}_{incident}$ (blue arrow); the dashed black line crosses each equifrequency contour in two points, but only one of these points identifies a wave vector inside the crystal that corresponds to a Bloch wave with positive $\mathbf{v}_g$ that can travel through the crystal. (f) Calculated field pattern using a Fourier imaging technique, based on the 3D equifrequency surface predicted by the MST. Adapted and extended from Refs. 4, 7 and 9.

is shown by the dashed blue curve, along with a representative incident wave vector $\mathbf{k}_{incident}$ that is inclined at a small angle away from the normal to the surface of the crystal. For a plane wave that is incident at this angle on the input face of the crystal at this frequency, the directions of the

wave vector $\mathbf{k}$ and the group velocity $\mathbf{v_g}$ for the corresponding Bloch waves inside the crystal are shown by the black arrows. These vectors must satisfy the following conditions. The direction of $\mathbf{k}$ is determined by the boundary conditions that the component of the wave vector parallel to the surface ($\mathbf{k}_{\text{par}} \perp \mathbf{k}_{\Gamma\text{L}}$) must be equal both inside and outside the crystal, according to Snell's law. Furthermore, for ultrasound to travel through the crystal, the direction of energy transport, which is given by $\mathbf{v}_g$ (and is the velocity of Bloch waves), must point in a positive direction, from the input to output surfaces of the crystal; its direction is perpendicular to the equifrequency surface, since $\mathbf{v}_g = \nabla_{\mathbf{k}}\omega(\mathbf{k})$. [Note that since the equifrequency contours become smaller as the frequency increases, the direction of $\mathbf{v}_g$ is inwards, as indicated by the representative $\mathbf{v}_g$ arrow in Fig. 1(e).] Thus, these conditions impose positive $\mathbf{v}_g$ and negative $\mathbf{k}$ in the first Brillouin zone, and lead directly to wave transport in a direction that corresponds to a *negative* angle of refraction (wave transport in the crystal on the *same* side of the normal to the surface as the incident wave). The schematic "ray" diagrams shown in Figs. 1(b) and 1(d) illustrate how this large negative refraction of Bloch waves inside the crystal leads to focusing of the ultrasonic waves on the far side of the crystal (and substrate); waves with incident angles $\pm\theta$ refract negatively on entering the crystal, cross inside the crystal, and refract negatively again on leaving the crystal, so that they are directed to a common focal point on the far side of the crystal. The very large anisotropy of the equifrequency surfaces near 1.6 MHz means that incoming waves at different angles of incidence are refracted through different angles inside the crystal, and therefore are brought to a focus at different distances on the far side of the crystal. While anisotropy therefore leads to images of the source that are elongated along the z direction perpendicular to the crystal surfaces – a drawback for imaging applications – the very large resulting negative refraction that occurs at small angles of incidence enables far field focusing, which can sometimes be an advantage, as noted in the observations reported in the previous paragraph.

The cross sections of the equifrequency surfaces shown in Fig. 1(e) show that the equifrequency surfaces become more isotropic as the frequency is increased above 1.6 MHz. While this decreased anisotropy might suggest that higher frequencies would be better for imaging, in fact the reverse is true in practice. To investigate the focusing at these higher frequencies in the same band, an identical 3D crystal was fabricated on a very thin substrate with longitudinal wave properties close to water. These experiments showed that the FWHM of the focal spot increased steadily from approximately 2λ at 1.6 MHz to around 10λ at 1.9 MHz. Thus the tranverse width of the focal spot becomes larger as the frequency increases, leading to poorer focusing; this effect that can be explained by the smaller size of the equifrequency surfaces, which reduce the range of incident angles from the source field that can be negatively refracted and subsequently focused.

To further elucidate the focusing mechanism, the shape of the focal spot was calculated using a Fourier imaging technique. In this approach, the spatial Fourier transform of the input beam from the source was calculated, thereby decomposing the input signal into plane waves, and then Snell's law and the equifrequency surfaces were used to determine how each plane wave component propagated through the crystal. In the detecting plane, the field pattern at focal spot was then calculated by taking an inverse Fourier transform back into real space. The results, at the frequency corresponding to the experimental image in Fig. 1(c), are shown in Fig. 1(f), which can be seen to be in excellent agreement with the experiment. The excellent agreement confirms that this model correctly incorporates the essential physics of this wave-focusing phenomenon. Thus the authors were able to determine directly the focusing mechanism and to show how this mechanism can be simply described in terms of negative refraction. It is nonetheless important to emphasize that, despite the similarities with negative refraction in doubly negative metamaterials,[3] where negative refraction arises from local resonances, the origin of negative refraction in phononic crystals is a band-structure effect; in both cases, the direction of energy transport due to negative refraction is determined by Poynting's vector, and for phononic crystals it is always given by the direction of the group velocity.[4]

III. DIRECT OBSERVATION OF NEGATIVE REFRACTION IN PHONONIC CRYSTALS

While this first focusing experiment in phononic crystals gave convincing evidence that negative refraction provided the actual focusing mechanism, this experiment did not provide a *direct* obsevation of negative refraction *per se*. However, it was not long before more direct observations

of negative refraction in phononic crystals were made via experiments, simulations and theoretical calculations.[9–16] These observations were made using 2D crystals, to take advantage of their relative simplicity compared with 3D. Most of these investigations of negative refraction used a slab-shaped sample, with a beam having a near-Gaussian transverse profile incident on one of the large parallel crystal surfaces at an angle (typically ranging from 6 to 30 degrees) away from the surface normal. Refraction of the incoming beam inside the crystal was deduced by measuring the transverse position of the most intense signal emerging on the opposite side of the slab, with the refraction being negative if the lateral shift of transmitted beam was found to be on the same side of the surface normal as the incident beam. The 2D crystal structure in these experiments was either triangular or square, with the most common configuration consisting of solid rods (e.g., steel) embedded in a fluid matrix (usually air or water). From the lateral shift of the transmitted beam, an effective negative refractive index could be determined; for example, Ke *et al.*[13] measured the frequency dependence of this negative refractive index over a wide frequency range in the second band of their phononic crystal, obtaining values between −0.9 and −0.3.

An even clearer method of observing negative refraction is to study refraction in a prism-shaped phononic crystal. In this case, positively or negatively refracted beams leaving the crystal can be seen to travel in completely different directions, in contrast to the slab geometry, where one has to measure transverse shifts of the emerging beam that are generally much smaller than the beam width. The experiments of Sukhovich *et al.*[15] capitalized on this approach using a prism to demonstrate negative refraction very convincingly. In this work, they performed a complete set of ultrasonic experiments on a phononic crystal that was fabricated in the shape of a right-angle prism with angles 30°, 60° and 90°. The crystal contained steel rods surrounded by water, with the rods arranged in a triangular lattice at a volume fraction of 58%. One of the attractive features of this crystal is its simple band structure,[13,15] which is shown in Fig. 2(a). Here, the solid curves are the predictions of Multiple Scattering Theory, and the symbols represent experimental results on a 6-layer-thick slab-shaped sample. The good range of frequencies to observe negative refraction effects is the second pass band, above the stop band along ΓM and below the band gap near 1 MHz, where there is only one branch, which, from its symmetry about the Γ point, appears to be isotropic. Detailed examination of the equifrequency contours, calculated using MST and shown for several frequencies in Fig. 2(b), confirm this isotropic behaviour, demonstrating that deviations from ideal circular contours are remarkably small, being significantly less than 1% for all frequencies between 0.69 MHz and the top of the band at 1.0 MHz.[15] Thus, the wave vector has the same magnitude in all directions, and since the contours shrink in size as the frequency increases, the group velocity $\mathbf{v_g}$ points towards the centre of each circular contour and is antiparallel to the wave vector in the first Brillouin zone. Thus, this condition that $\mathbf{v_g}$ and $\mathbf{k}$ are antiparallel in this band is the same as that found for left-handed behaviour in negative index metamaterials,[3] so that waves arriving at the surface of the crystal at non-normal incidence are expected to experience negative refraction. Experimental evidence that this is indeed the case is presented in Fig. 2(c). In this experiment, a narrowband pulse with a central frequency of 0.85 MHz was incident on the shortest face of the prism with its direction of propagation perpendicular to this face (see the wide blue arrow) and the field that emerged from the longest face was mapped out by scanning a miniature hydrophone in a high-resolution grid pattern. Inside the crystal, the pulse continued to travel in the direction of incidence, parallel to the group velocity, since it arrived at the crystal at normal incidence. The prediction from the equifrequency contours that the wave vector $\mathbf{k}_c$ inside the crystal points backwards, opposite to the group velocity, was verified experimentally by the negatively refracted outgoing field pattern, which bends backwards in the negative direction, applying Snell's law at the interface through which the waves leave the crystal to relate the wave vector inside the crystal to the measured wave vector outside. In Fig. 2(c) this point is emphasized by indicating the directions of the Bloch wave vector and group velocity inside the crystal, as well as the direction of $\mathbf{k}_w$ for the refracted beam in the water outside, which is perpendicular to the wave fronts. Furthermore, the refraction angle θ_w was measured to be $-21° \pm 1°$ in excellent agreement with the theoretical prediction of −20.4°, based on Snell's law and the calculated value from MST of the wave vector inside the crystal, thereby showing convincingly that the data can be quantitatively described in terms of negative refraction. It is also worth pointing out that to measure the direction of $\mathbf{k}$ precisely, it is crucial to measure the wave field and not just the intensity so that $\mathbf{k}$ can be

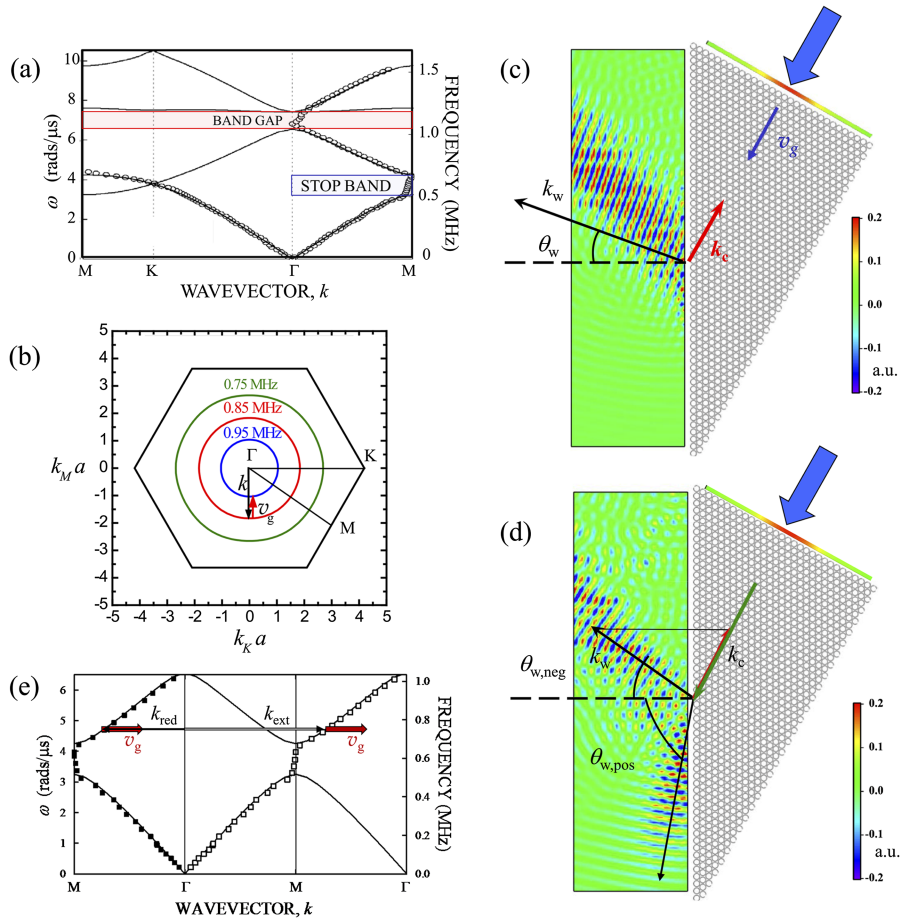

FIG. 2. (a) Comparison of theoretical and experimental results for the band structure of a phononic crystal of 1.02-mm-diameter rods steel rods in water, configured in a triangular lattice with lattice constant a = 1.27 mm. The solid curves were calculated using Multiple Scattering Theory, and the symbols represent experimental data. (b) Equifrequency contours at frequencies 0.75, 0.85 and 0.95 MHz in the second pass band, calculated with MST. (c) Snapshot of the negatively-refracted wave pulse emerging from a phononic crystal prism after a narrow-band pulse with a central frequency of 0.85 MHz was normally incident on the shortest face of the prism (in the direction of wide blue arrow). The data were acquired using a broadband input pulse and measuring the transmitted field, point by point, over a rectangular grid with a subwavelength diameter hydrophone. The data were then digitally filtered to obtain results for a narrow range of frequencies, and the wave field at a particular moment in time was measured to construct the spatial variation of the field at that time. The directions of the group velocity and wave vector inside the crystal, as well as the wave vector of the refracted beam outside, are shown by the arrows. (d) Snapshot of the refracted waves at 0.75 MHz, showing both negatively and positively refracted waves. (e) Measured and calculated band structures along the ΓM direction displayed in the reduced zone (solid symbols, left side) and extended zone (open symbols, right side) schemes. The wide shorter red arrows indicate the direction of the group velocity, while the narrower black arrows indicate the wave vectors. Adapted from Refs. 15 and 23.

determined from the wave fronts, as the position of maximum intensity in the refracted beam in this pulsed experiment is also influenced by the time taken for the pulse to reach the exit surface of the crystal, with the earlier arrivals being closer to the top of the prism and corresponding to the signals on the top left part of the measurement area.

Additional evidence of negative refraction in this crystal was obtained by performing the reciprocal experiment to the one shown in Fig. 2(c). By interchanging the generating and detecting transducers, and sending an incoming beam towards the large face of the prism in a direction that is opposite to that of the emerging beam in Fig. 2(c), the incoming beam was first refracted negatively as it entered the crystal and was then observed to emerge perpendicular to the smallest face of the prism. Again, the experimental results were in excellent agreement with theoretical predictions using the MST.

At lower frequencies in the same band [e.g., at 0.75 MHz, see Fig. 2(d)], in addition to the negatively refracted beam, a positively refracted beam was also observed emerging from the same face of the prism, and could be clearly distinguished since its direction of travel was on the opposite side of the surface normal.[15] This positively refracted beam was associated with the plane wave component of the Bloch wave inside the crystal having wave vector in the second Brillouin zone, for which $\mathbf{v_g}$ and $\mathbf{k}$ point in the same direction [Fig. 2(e)]. As at 0.85 MHz, excellent agreement between experiment and theory was found for the refraction angles: for the negative refraction case, the measured and predicted angles are $\theta_{w,neg} = -34^\circ \pm 1^\circ$ and $\theta_{w,neg} = -35.0^\circ$, while for the positive refraction case, the measured and predicted angles are $\theta_{w,pos} = 81^\circ \pm 1^\circ$ and $\theta_{w,pos} = 81.6^\circ$. As an aside, it may be interesting to note that this refraction experiment allows the two shortest wave vectors of the plane wave decomposition of the Bloch wave inside the crystal to be measured with the help only of Snell's law. However, this was not possible at 0.85 MHz, since in this case total internal reflection prevented this second plane wave component of the Bloch wave from escaping from the crystal, and only the negatively refracted beam could leave the crystal and be detected. Overall, it can be concluded that a consistent picture of refraction effects in this crystal was obtained, and clear evidence for negative refraction with $\mathbf{v_g}$ opposite to $\mathbf{k}$ in the first Brillouin zone was established.

For the triangular lattice considered in the previous example, wave propagation is isotropic throughout almost all of the second band, which is advantageous for focusing applications (see Sec. IV). By contrast, the square lattice is anisotropic, which can lead to rather rich refraction phenomena. For example, Bucay et al showed that, for a square array of polyvinylchoride rods in air, either positive, negative or zero refraction could be observed depending on the angle of incidence of the incoming beam.[16]

The observations of negative refraction discussed so far in this article were made almost entirely in phononic crystals constructed by embedding solid inclusions (steel or polyvinylchloride) in a fluid matrix (water or air). For practical applications, solid phononic crystals are generally more convenient. In this case, elastic waves with longitudinal or transverse polarizations can propagate. Negative refraction has been studied both numerically and experimentally in a relatively simple solid-solid phononic crystal consisting of steel rods embedded in an epoxy host and arranged in a triangular lattice.[17–20] This has allowed negative refraction of both longitudinal and transverse waves in prism-shaped crystals to be observed and thoroughly characterized. By demonstrating the negative refraction of longitudinal waves in this crystal system, the possibility of designing solid flat lenses for imaging systems in fluid environments was highlighted.[19]

IV. FOCUSING IN 2D PHONONIC CRYSTALS AND THE SEARCH FOR SUPER-RESOLUTION

Focusing of acoustic waves from point-like sources was also shown using flat lenses made from the 2D phononic crystals discussed in section III. In some cases, a focusing transducer was used to create the source,[13] implying that the range of incident angles was limited by the directivity pattern of the generating transducer. In another case, an absorbing waveguide was used to restrict the angular divergence of the beam from the generating transducer.[12] These demonstrations of focusing by negative refraction allowed the focusing condition that is shown in Fig. 1(d), $d_1 + d_2 = \beta L$, where $\beta = |\tan\theta_r / \tan\theta_i|$, to be examined. Here, d_1 and d_2 are the distances from the crystal to the source and detector, respectively, L is the crystal thickness, and θ_i and θ_r are the angles of incidence and refraction. Good overall agreement was found between experiments, simulations and theoretical predictions.

A particularly interesting structure that exhibits good focusing properties is the single metallic foam-like phononic crystal often referred to as metal water.[21] This structure owes its name to the fact that it is an aluminum-based metallic foam with an effective density and bulk modulus equivalent to water in the long wavelength limit. This phononic crystal has a negative band that includes a frequency with corresponding wave vector equal in magnitude to that of water. Finite element simulations and experiments showed that when a flat slab of this crystal is placed in a water bath and insonified with a point-like source, the half-width of the focal spot that forms on the opposite side of the crystal is predicted to be 0.53 λ and measured experimentally to be around 0.8 λ at a similar frequency. Here λ is the wavelength in water at the frequency for which the focal spot is narrowest.[21] It was concluded

that this flat phononic crystal lens could potentially be useful for imaging in a fluid or fluid-like medium, which is a situation encountered in medical imaging.

To investigate the best possible image resolution that may be achieved with a flat lens made from a 2D phononic crystal, it is instructive to return to the structure examined in Fig. 2, namely a triangular lattice of steel rods immersed in a fluid and surrounded by water. To this end, experiments were performed on a slab-shaped six-layer thick crystal of steel rods with the identical crystal structure and lattice parameters (1.02-mm-diameter rods and lattice constant 1.27 mm).[15] To avoid edge effects, each layer contained 60 rods, and the layers were arranged so that the ΓM direction was perpendicular to the layers. The initial focusing experiments were performed with water as the fluid both inside and outside the crystal, as for the negative refraction experiments shown in Fig. 2. An image of the focused field pattern obtained using the pinducer as the source, which was placed 2.5 mm from the crystal, is shown in Fig. 3(a). The positions of the rods at the surface of the crystal (on the side opposite the source) are shown by the black circles below the image, and the frequency is 0.75 MHz – the same as for the refraction experiments reported in Fig. 2(d). While the focal pattern is clearly confined along both the longitudinal (z) and transverse (x) directions, the depth of field of the focus is much longer than the transverse width. This elongation of the image of the source along the z direction is due to the imperfect match in radius of the crystal and water equifrequency contours, which give an *effective* refractive index of -0.66, so that, despite the excellent circularity of the crystal equifrequency contours, incident waves at different angles of incidence are brought to a focus at different distances from the crystal surface. To assess the lateral resolution of the image, the transverse profile of the image along a line parallel to the crystal surface and through the image maximum was measured and fitted by the sinc function $|\sin(2\pi x/\Delta)/(2\pi x/\Delta)|$, where Δ is the distance between the first zeroes on either side of the maximum and represents the full width of the peak. According to the Rayleigh criterion, the resolution is $\Delta/2$, giving a resolution of 1.26λ at this frequency, where λ is the wavelength in water. Thus, this resolution is well beyond the diffraction limit of $\lambda/2$, due to the poor

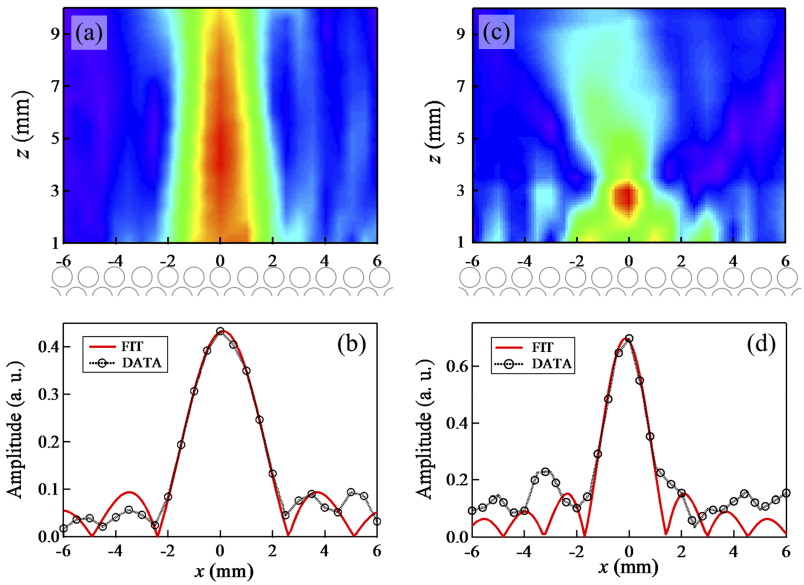

FIG. 3. Contour plots, and cross sections along a line parallel to the crystal surface and through the focal point, of the experimentally measured field amplitude (magnitude of the FFT of the ultrasonic wave field at a given frequency) transmitted through flat phononic crystal lenses when a pinducer source was placed near the opposite surface. (a): Image measured at 0.75 MHz when the phononic crystal consisted of 6 layers of steel rods, arranged in a triangular lattice and immersed in water. The source-lens distance was 2.5 mm. (b): Amplitude parallel to the lens surface (open circles) through the focus in (a). The data are compared with a sinc function (red curve), indicating a resolution $\Delta/2 = 1.26\lambda$. (c): Image measured at 0.55 MHz when the water in the phononic crystal was replaced by methanol. The source-lens distance was 2 mm. (d): Comparison of experimental results for the transverse width of the focal spot (c) (circles) with a fitted sinc function (red curve). In this case the image resolution is 0.58λ. Adapted from Refs. 15 and 23.

matching of the equifrequency contours, which limit the range of incident angles that can be refracted to those below 42° and therefore eliminate the large transverse wavevectors needed to capture small size information. By going to lower frequencies, the resolution can be somewhat improved, as the equifrequency contours of the crystal equifrequency contours only remain circular (within 1%) down to 0.69 MHz, but the best resolution that can be achieved at this frequency is only 1.1λ.

The focusing example in Figs. 3(a) and 3(b) show very clearly that good focusing approaching the diffraction limit is not possible unless the equifrequency contours inside and outside the crystal are equal. To enable this condition to be met with a steel rod crystal, a new sample was built with thin transparent walls so that the water surrounding the rods inside the crystal could be replaced with a lower velocity liquid. The new liquid chosen was methanol ($v_{\text{methanol}} = 1.14$ mm/μs), which has a lower sound velocity than water ($v_{\text{water}} = 1.49$ mm/μs), shrinking the frequency axis of the bandstructure shown in Fig 2(a) by 74%. As a result, at a frequency of 0.55 MHz and wave vector that is well inside in the second band (84% of the maximum wave vector at the Brillouin zone boundary), the equifrequency contours of both the crystal and the water outside were perfectly matched. Thus, at this frequency, the effective refractive index is −1, and all angle negative refraction (AANR) was achieved. The AANR condition also holds for all other frequencies down to the bottom of the band at 0.50 MHz. The image obtained at 0.55 MHz, using the same pinducer source, is shown in Fig. 3(c). A greatly improved focal pattern is clearly seen, with the focal spot narrowly confined both perpendicular and parallel to the crystal surface. Again, a sinc function gives a good description of the transverse width of the focal spot, allowing the full width and resolution to be determined as 3.16 mm and 0.58λ, respectively (Fig. 3(d)). This result shows that a flat phononic crystal with equifrequency contours equal to those of the medium outside can produce images with an excellent resolution approaching the diffraction limit.[15,22,23]

To explore the possibility of achieving even better resolution with this flat methanol-filled phononic crystal, an important first step was to replace the pinducer by a narrow line source with a subwavelength width of 0.55 mm. This width is much less than the wavelength in water at the relevant frequencies for focusing with this crystal, which are of order 3 mm. The new source transducer was constructed from piezoelectric polymer strips. The improvement in resolution using the line source was quite slight, however, when a comparable source-lens distance of 1.6 mm was used, with the resulting resolution being $\Delta/2 = 0.55\lambda$.[15]

To achieve super resolution (better than the diffraction limit), it is necessary to capture and amplify evanescent waves from the source. It was discovered that when the narrow line source was brought extremely close to the surface of the crystal, 0.1 mm or $\lambda/25$ away, the resolution was significantly improved,[24] as shown by the results presented in Fig. 4. The field amplitude map in Fig. 4(a), which was obtained from a Finite Difference Time Domain (FDTD) simulation of the acoustic pressure field both inside and outside the crystal, shows that, at this very small source-crystal separation, the entire crystal "lights up" due to the excitation of a bound slab mode of the crystal. When the source is close enough, this bound mode can couple to some of the evanescent waves from the source, allowing a significant component of the evanescent field to become amplified sufficiently to participate in the formation of the image. Evidence for the evanescent character of this mode can be seen from the field maps in Figs. 4(a)–4(c), where additional peaks on both sides of the focal spot are seen in the field pattern close to the crystal surface at $z = 0$; these peaks decay rapidly with distance from the crystal surface, as expected for the evanescent decay of bound modes. The best resolution of the focal spot was found at a frequency of 0.53 MHz that is slightly lower that the optimum frequency for equifrequency contour matching, as was shown by analysis of the field maps. Results at 0.53 MHz, zoomed in near the focal spot for both experiments and simulations, are presented in Figs. 4(b) and 4(c), respectively, and the comparison of experiment and simulation for the transverse and longitudinal profiles is shown in Figs. 4(d) and 4(e). There is good agreement between the experimental and simulation results, and both show clearly that the measured resolutions of 0.37λ in experiment and 0.35λ in simulation are better than the diffraction limit. Additional information on the bound mode, which is responsible for the observed super resolution, was obtained from calculations of the band structure, using FDTD method, of a *finite* 6-layer crystal slab (i.e., with same number of layers as the experimental crystal).[24] These band structure calculations in the finite crystal revealed the existence of a nearly flat band, corresponding to propagation along the direction parallel to the

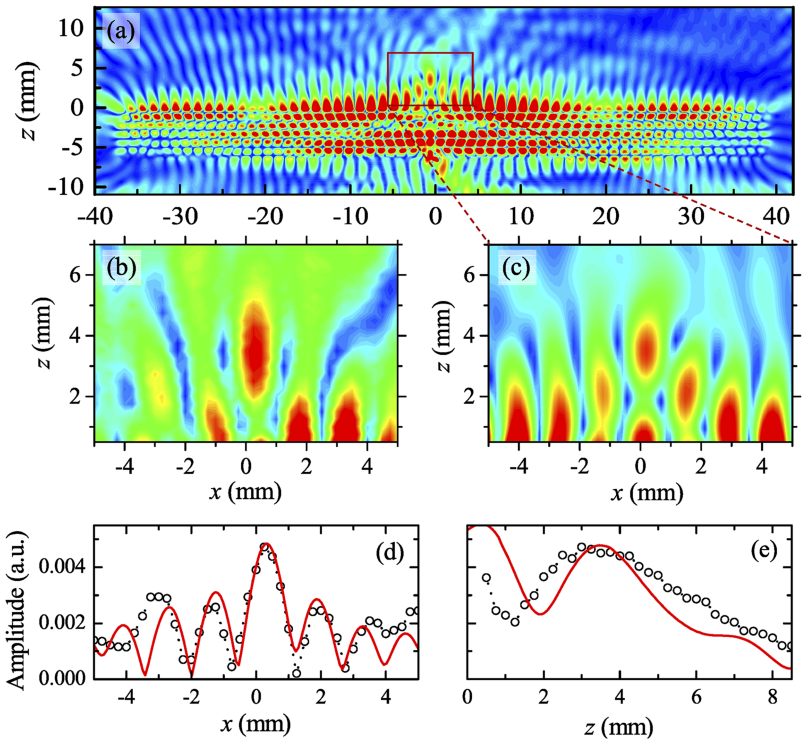

FIG. 4. (a)-(c): Contour maps of the magnitude of the ultrasonic pressure field when a subwavelength 0.55-mm-wide line source was placed in front of one of the rods of the flat methanol-steel phononic crystal lens at a distance of only 0.1 mm. In (a), a FTDT simulation of the pressure field both inside and outside the entire crystal is displayed, showing the bound mode that is excited when the source-lens distance is so small. The bound mode extends over the whole crystal and decays evanescently outside. The frequency is 0.53 MHz. The source is located near the lower surface of the crystal at $x = 0$ and $z = -6.6$ mm, and is centered with respect to a rod. The upper surface of the crystal is at z = 0. The contours in (b) and (c) compare experiment and simulation, respectively, for the field amplitude near the focal spot. (d) and (e): Comparison of experiment (open circles) and simulations (red curves) for the transverse width of the focal spot (d) and its variation with distance from the surface of the crystal (e). The narrow widths of the primary peaks correspond to resolutions of 0.37λ and 0.35λ for the experiments and simulations, respectively. Adapted from Ref. 24.

surface (ΓK), that lies below the water line, so that these excitations are bound to the crystal slab since they cannot propagate in water. This almost flat band varies in frequency between 0.525 and 0.51 MHz between its intersection with water line and the K point at the zone boundary. The reason that the best focusing is seen at 0.53 MHz is now easy to understand, as this frequency represents the best compromise between the frequency for perfectly matched equifrequency contours (0.55 MHz) and the resonance frequencies of the bound mode (0.51 - 0.525 MHz). Fortuitously, 0.53 MHz is still sufficiently close to the bound mode frequency band that the bound mode can be excited. It is also worth emphasizing that the FDTD calculations show that the field pattern inside the phononic crystal corresponds to a bulk bound mode of the crystal slab, and not a surface mode; thus, transverse wave vectors up to the K point of the bulk Brillouin zone may be eligible to assist with the formation of an image. This implies that a larger range of evanescent wave vectors from the source can couple to the bound mode than would be the case if only wave vectors up to the X point of the surface Brillouin zone were involved, enabling a better resolution to be achieved than would be possible if the surface mode mechanism originally considered by Luo et al. for photonic crystals were responsible.[25]

This demonstration of super resolution focusing of the field from a quasi-point source using a phononic crystal has enabled the many factors that can influence the optimum resolution to be investigated in considerable detail.[24,26] For example, it was shown that the lateral placement of the source parallel to the phononic crystal lens surface is very important for achieving super resolution, since the source must be placed in a position where the bound mode can be efficiently excited; for this lens, optimum focusing occurs when the source is centered on one of the rods,

and super resolution disappears when the source is placed halfway between the rods, where the bound mode displacement field has a node. Other factors include the distance from the source to the lens (the lens must be very close to the source for super resolution to be possible), the relationship between image distance and source distance from the lens surface, the choice of best operating frequency (discussed in the previous paragraph), the bandwidth over which super resolution can be realized (nearly 10%), the effect of varying the thickness of the lens on image resolution, the time required for optimum resolution to be reached, and the detrimental effect of lattice disorder. Perhaps the most interesting question concerns the mechanism that determines the resolution limit for imaging with this phononic crystal lens. This limit is set by the largest transverse wave vector k_{max} that the crystal will support, which is expected to be the wave vector at the Brillouin zone boundary of the crystal along the ΓK direction (parallel to the surface of the lens).[26] This condition gives $k_{max} = 4\pi/3a$. The resolution limit can be estimated using a simple model in which perfect transmission is assumed for all transverse wave vectors $k_{par} < k_{max}$ and zero transmission for $k_{par} > k_{max}$. This model then predicts that the variation of the image amplitude with distance x parallel to the crystal surface is

$$\left| \int_{-k_{max}}^{k_{max}} \exp\left[ik_{par}x\right] dk_{par} \right| = \left|2\sin\left(k_{max}x\right)/\left(k_{max}x\right)\right| .$$

Hence, the predicted resolution limit $\Delta_{min}/2$ is $\pi/k_{max} = 3a/4$, giving $\Delta_{min}/2 = 0.34\lambda$ at 0.53 MHz. This prediction is very close to the experimental and FDTD simulation results.

These experimental and theoretical results on focusing by negative refraction in a simple phononic crystal of stainless steel rods immersed in methanol demonstrate how optimal focusing can be achieved. The main conditions that need to be satisfied are:

(i) the equifrequency surfaces should be spherical in 3D, and the equifrequency contours should be circular in 2D,
(ii) well matched equifrequency surfaces (or contours) in the phononic crystal and in the medium outside are essential, so that the effective negative index of refraction is -1, and,
(iii) a flat band of bound modes at frequencies close to the operational frequency is needed for super resolution to be attained, so that amplification of evanescent waves from the source can occur.

These conditions are relevant for designing any other type of phononic crystal lens in which super resolution may even be enhanced.

One possibility for achieving better resolution could be to retain the same crystal structure of steel rods surround by a fluid, but to replace the methanol with an even lower velocity medium. This would shift the equifrequency matching condition with the water medium surrounding the crystal to a lower frequency, which could favor improved resolution. The finite element simulations shown in Fig. 5 indicate that if the methanol is replaced with fluorinert, for which the velocity is 0.525 mm/μs, the resolution of the image of a point source at the frequency 0.318 MHz becomes 0.25λ. This prediction of enhanced resolution remains to be tested experimentally.

Another approach for achieving super resolution of a 2D phononic crystal of rods in water was proposed by He *et al.*, who added a surface modulation to a square lattice of rubber-coated tungsten cylinders in order to induce acoustic surface waves on the crystal.[27] This surface modulation was shown by numerical simulations to produce surface states that amplified evanescent waves from the source, leading to a resolution of 0.35λ, which is again smaller than the diffraction limit of 0.5λ. Inspired by developments in elastic metamaterials,[28] Zhou et al. have predicted superlensing for acoustic waves in water using a solid 2D phononic crystal containing a complex unit cell of four heavy cylinders surrounding a cylindrical cavity embedded in an elastically weak Al-SiC foam matrix.[29] They showed that this structure has surface states that can couple to and amplify evanescent waves from a point-like source in water, leading to a spatial resolution of 0.41λ. It was pointed out that the solid nature of the proposed lens would be an advantage for imaging applications.

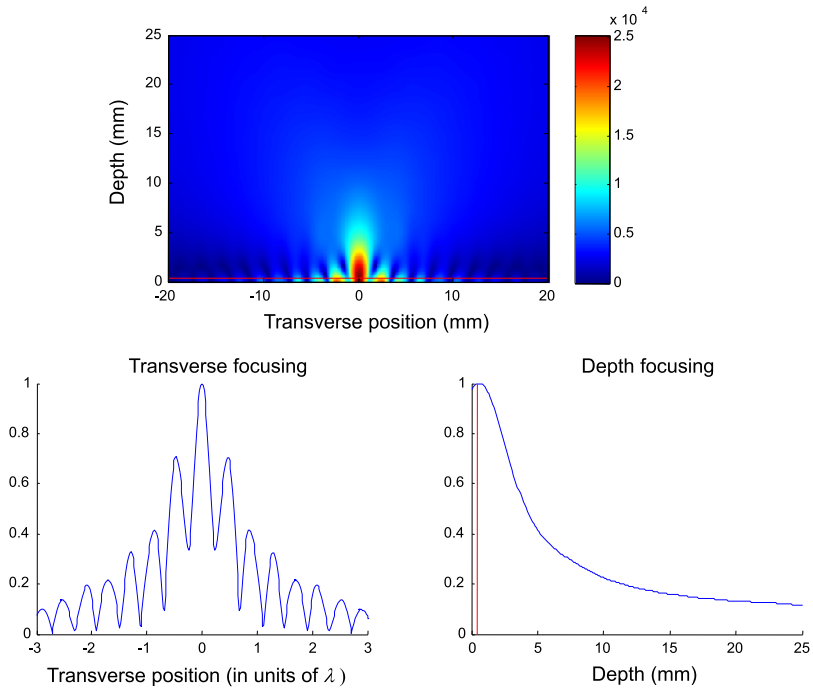

FIG. 5. Image of a point source that is formed on the opposite side of a phononic crystal of steel rods immersed in fluorinert.

V. CONCLUSIONS AND OUTLOOK

This paper summarizes research activities that have taken place over the last almost 15 years on negative refraction in phononic crystals and its use in the development of flat phononic crystal lenses. Following the initial demonstration of focusing ultrasonic waves by negative refraction,[4] many groups have investigated and further developed phononic crystal lenses that exploit negative refraction using a variety of materials and approaches.[5–24,26–28] There have also been very significant parallel advances in focusing studies with Lamb waves and surface acoustic waves,[30–38] and other types of flat lenses for acoustic waves (e.g., GRIN lenses[34,38–40]). A related area is negative refraction and/or imaging with acoustic and elastic metamaterials,[28,41–58] where there has already been very significant progress and promise of increasing interest in the future. The possibility of creating deeply subwavelength doubly-negative metamaterials is leading to very significant advances in superlensing; one example is the realization of a negative index acoustic metamaterial based only on Helmholtz resonators, in which subwavelength focusing and imaging has been demonstrated with a spot width and resolution that are respectively 7 and 3.5 times better that the diffraction limit.[57] This example shows the great potential of acoustic metamaterials to enable focusing and imaging with greatly enhanced super resolution. While a wide range of potential applications of negative refraction focusing has been suggested in many of the papers cited in this review, they appear to remain largely unrealized so far; these proposed applications include enhanced imaging for medical diagnoses, sonar and ultrasonic non-destructive evaluations, and even novel micromechanical actuators and sensors.

ACKNOWLEDGMENTS

Support from NSERC's Discovery Grant Program is gratefully acknowledged. I would like to thank Fabrice Lemoult for performing the finite element simulations shown in Fig. 5.

[1] B. Taylor, H. J. Maris, and C. Elbaum, Phys. Rev. Lett. **23**, 416 (1969).
[2] J. P. Wolfe, *Imaging Phonons: Acoustic Wave Propagation in Solids* (Cambridge University Press, Cambridge, U.K., 1998).
[3] J. B. Pendry, Phys. Rev. Lett. **85**, 3966 (2000).
[4] S. Yang, J. H. Page, Z. Liu, M. L. Cowan, C. T. Chan, and P. Sheng, Phys. Rev. Lett. **93**, 024301 (2004).
[5] A. Sukhovich and J. H. Page, in *2006 McGraw-Hill Yearbook of Science and Technology* (2006), pp. 230–233.

[6] A. Sukhovich, J. H. Page, J. O. Vasseur, J. F. Robillard, N. Swintek, and P. A. Deymier, in *Phononic Crystals and Acoustic Metamaterials*, edited by P. Deymier (Springer Series in Solid-State Sciences, Berlin Heidelberg, 2013), pp. 95–158.
[7] S. Yang, J. H. Page, Z. Liu, M. L. Cowan, C. T. Chan, and P. Sheng, Phys. Rev. Lett. **88**, 104301 (2002).
[8] Z. Liu, C. T. Chan, P. Sheng, A. L. Goertzen, and J. H. Page, Phys. Rev. B **62**, 2446 (2000).
[9] J. H. Page, A. Sukhovich, S. Yang, M. L. Cowan, F. Van Der Biest, A. Tourin, M. Fink, Z. Liu, C. T. Chan, and P. Sheng, Phys. Stat. Sol. (b) **241**(15), 3454 (2004).
[10] X. Zhang and Z. Liu, Appl. Phys. Lett. **85**, 341 (2004).
[11] L. Feng, X.-P. Liu, Y.-B. Chen, Z. P. Huang, Y.-W. Mao, Y. F. Chen, J. Zi, and Y. Y. Zhu, Phys. Rev. B **72**, 033108 (2005).
[12] L. Feng, X.-P. Liu, M.-H. Lu, Y.-B. Chen, Y.-F. Chen, Y.-W. Mao, J. Zi, Y. Y. Zhu, S. N. Zhu, and N. B. Ming, Phys. Rev. Lett. **96**, 014301 (2006).
[13] M. Ke, Z. Liu, C. Qiu, W. Wang, J. Shi, W. Wen, and P. Sheng, Phys. Rev. B **72**, 064306 (2005).
[14] M.-H. Lu, C. Zhang, L. Feng, J. Zhao, Y.-F. Chen, Y.-W. Mao, J. Zi, S. N. Zhu, and N. B. Ming, Nat. Materials **6**, 744 (2007).
[15] A. Sukhovich, L. Jing, and J. H. Page, Phys. Rev. B **77**, 014301 (2008).
[16] J. Bucay, E. Roussel, J. O. Vasseur, P. A. Deymier, A.-C. Hladky-Hennion, Y. Pennec, K. Muralidharan, B. Djafari-Rouhani, and B. Dubus, Phys. Rev. B **79**, 214305 (2009).
[17] B. Morvan, A. Tinel, A.-C. Hladky-Hennion, J. O. Vasseur, and B. Dubus, Appl. Phys. Lett. **96**, 101905 (2010).
[18] A.-C. Hladky-Hennion, C. Croënne, B. Dubus, J. O. Vasseur, L. Haumesser, D. Manga, and B. Morvan, AIP Advances **1**, 041405 (2011).
[19] C. Croënne, D. Manga, B. Morvan, A. Tinel, B. Dubus, J. O. Vasseur, and A.-C. Hladky-Hennion, Phys. Rev. B **83**, 054301 (2011).
[20] D. Manga, B. Morvan, E. le Clésio, and A.-C. Hladky-Hennion, *2011 IEEE International Ultrasonics Symposium Proceedings*, 2491 (2011).
[21] A.-C. Hladky-Hennion, J. O. Vasseur, G. Haw, C. Croënne, L. Haumesser, and A. N. Norrris, Appl. Phys. Lett. **102**, 144103 (2013).
[22] P. A. Deymier, B. Merheb, J. O. Vasseur, A. Sukhovich, and J. H. Page, Revista Mexicana de Fisica S **54**, 74 (2008).
[23] A. Sukovich, Ph.D. thesis, University of Manitoba (2007).
[24] A. Sukhovich, B. Merheb, K. Muralidharan, J. O. Vasseur, Y. Pennec, P. A. Deymier, and J. H. Page, Phys. Rev. Lett. **102**, 154301 (2009).
[25] C. Luo, S. G. Johnson, J. D. Joannopoulos, and J. B. Pendry, Phys. Rev. B **68**, 045115 (2003).
[26] J. F. Robillard, J. Bucay, P. A. Deymier, A. Shelke, K. Muralidharan, B. Merheb, J. O. Vasseur, A. Sukhovich, and J. H. Page, Phys. Rev. B **83**, 224301 (2011).
[27] Z. He, X. Li, J. Mei, and Z. Liu, Appl. Phys. Lett. **106**, 026105 (2009).
[28] Y. Lai, Y. Wu, P. Sheng, and Z.-Q. Zhang, Nat. Mater. **10**, 620 (2011).
[29] M. Zhou, M. B. Assouar, and M. Oudich, Appl. Phys. Lett. **105**, 233506 (2014).
[30] J. Pierre, O. Boyko, L. Belliard, J. O. Vasseur, and B. Bonello, Appl. Phys. Lett. **97**, 121919 (2010).
[31] I. A. Veres, T. Berer, O. Matsuda, and P. Burgholzer, J. Appl. Phys. **112**, 053504 (2012).
[32] S. Bramhavar, C. Prada, A. A. Maznev, A. G. Every, T. B. Norris, and T. W. Murray, Phys. Rev. B **83**, 014106 (2011).
[33] M. A. Al-Lethawe, M. Addouche, A. Khelif, and S. Guenneau, New J. Phys. **14**, 123030 (2012).
[34] T. T. Wu and C.-W. Chen, *2012 IEEE International Ultrasonics Symposium* 1 (2012).
[35] M. Dubois, M. Fahrat, E. Bossy, S. Enoch, S. Guenneau, and P. Sebbah, Appl. Phys. Lett. **103**, 071915 (2013).
[36] H. Jia, M. Lu, Q. Wang, M. Bao, and X. Li, Appl. Phys. Lett. **103**, 103505 (2013).
[37] M. Addouche, M. A. Al-Lethawe, A. Choujaa, and A. Khelif, Appl. Phys. Lett. **105**, 023501 (2014).
[38] J. F. Zhao, R. Marchal, B. Bonello, and O. Boyko, Appl. Phys. Lett. **101**, 261905 (2012).
[39] V. Romero-García, A. Cebrecos, R. Picó, V. J. Sánchez-Morcillo, L. M. Garcia-Raffi, and J. V. Sánchez-Pérez, Appl. Phys. Lett. **103**, 264106 (2013).
[40] V. M. Garcia-Chocano, J. Christensen, and J. Sánchez-Dehesa, Phys. Rev. Lett. **112**, 144301 (2014).
[41] J. Li and C. T. Chan, Phys. Rev. E **70**, 055602 (2004).
[42] N. Fang, D. Xi, J. Xu, M. Ambati, W. Srituravanich, C. Sun, and X. Zhang, Nat. Mater. **5**, 452 (2006).
[43] Y. Ding, Z. Liu, C. Qiu, and J. Shi, Phys. Rev. Lett. **99**, 093904 (2007).
[44] M. Ambati, N. Fang, C. Sun, and X. Zhang, Phys. Rev. B **75**, 195447 (2007).
[45] D. Torrent and J. Sánchez-Dehesa, New J. Phys. **69**, 323 (2007).
[46] J. Li, L. Fok, X. Yin, G. Bartal, and X. Zhang, Nat. Mater. **8**, 931 (2009).
[47] F. Liu, F. Cai, S. Peng, M. Hao, M. Ke, and Z. Liu, Phys. Rev. E **80**, 026603 (2009).
[48] S. Zhang, L. Yin, and N. Fang, Phys. Rev. Lett. **102**, 194301 (2009).
[49] J. Zhu, J. Christensen, J. Jung, L. Martin-Moreno, X. Yin, L. Fok, X. Zhang, and F. J. Garcia-Vidal, Nat. Phys. **7**, 52 (2011).
[50] F. Lemoult, M. Fink, and G. Lerosey, Phys. Rev. Lett. **107**, 064301 (2011).
[51] L. Fok and X. Zhang, Phys. Rev. B **83**, 214304 (2011).
[52] J. Christensen and F. J. G. de Abajo, Phys. Rev. Lett. **108**, 124301 (2012).
[53] D. Bigoni, S. Guenneau, A. B. Movchan, and M. Brun, Phys. Rev. B **87**, 174303 (2013).
[54] X. Zhou, M. B. Assouar, and M. Oudich, J. Appl. Phys. **116**, 194501 (2014).
[55] R. Zhu, X. N. Liu, G. K. Hu, C. T. Sun, and G. L. Huang, Nat. Commun. **5**, 5510 (2014).
[56] T. Brunet, A. Merlin, B. Mascaro, K. Zimny, J. Leng, O. Poncelet, C. Aristégui, and O. Mondain-Monval, Nat. Mater. **14**, 384 (2015).
[57] N. Kaina, F. Lemoult, M. Fink, and G. Lerosey, Nature **525**, 77 (2015).
[58] S. A. Cummer, J. Christensen, and A. Alù, Nature Reviews Materials **1**, 16001 (2016).